Active vibration control of a doubly curved composite shell stiffened by beams bonded with discrete macro fibre composite sensor/actuator pairs

Ali H. Daraji
Faculty of Engineering, Environment and Computing, Coventry University, UK
e-mail: ac7202@coventry.ac.uk
ASME Membership (102081192)

Jack M. Hale
School of Mechanical and Systems Engineering, Newcastle University, UK
e-mail: jack.hale@ncl.ac.uk

Jianqiao Ye
Engineering Department, Lancaster University, UK
e-mail: j.ye2@lancaster.ac.uk

ABSTRACT

Doubly curved stiffened shells are essential parts of many large-scale engineering structures, such as aerospace, automotive and marine structures. Optimisation of active vibration reduction has not been properly investigated for this important group of structures. This study develops a placement methodology for such structures under motion base and external force excitations to optimise the locations of discrete piezoelectric sensor/actuator pairs and feedback gain using genetic algorithms for active vibration control. In this study, fitness and objective functions are proposed based on the maximization of sensor output voltage to optimise the locations of discrete sensors collected with actuators to attenuate several vibrations modes. The optimal control feedback gain is determined then based on the minimization of the linear quadratic index. A doubly curved composite shell stiffened by beams and bonded with discrete piezoelectric sensor/actuator pairs is modelled in this paper by first-order shear deformation theory using finite element method and Hamilton's principle. The proposed methodology is implemented first to investigate a cantilever composite shell to optimise four sensor/actuator pairs to attenuate the first six modes of vibration. The placement methodology is applied next to study a complex stiffened composite shell to optimise four sensor/actuator pairs to test the methodology effectiveness. The

results of optimal sensor/actuator distribution are validated by convergence study in genetic algorithm program, ANSYS package and vibration reduction using optimal linear quadratic control scheme.

Keywords, sensor, composite, stiffened shell, base excitation, genetic algorithms, vibration control

1. INTRODUCTION

High specific strength plates and shells stiffened by beams have been intensively used in aerospace, hydrospace and automotive structures to optimise loading capacity, energy consumption and material cost. These structures are flexible with low damping and may operate under external disturbance at resonance frequencies that may cause undesirable severe vibrations, lose energy and eventually damage the structures. These vibrations are mostly reduced passively by adding masses and dampers or actively by integrating a smart lightweight piezoelectric material with the main structure. Active vibration control offers great potential for an aerospace application using the lightweight piezoelectric material as sensors and actuators that can detect and efficiently reduce low energy structural vibration. The first study to formulate the dynamic equation for piezoelectric electro-elasticity was proposed by Allik and Hughes using finite element and variational methods [1]. Active vibration control of flexible structures bonded with full coverage of piezoelectric sensor/actuator pairs was modelled and investigated thoroughly in [2]-[7]. Active vibration control of composite shells was examined by Kulkarni and Bajoria who found that the optimal damping was obtained at a coverage of 50% of the structure by a piezoelectric material and it declined when the coverage was above 60% [4]. Lim studied vibration control of clamped plates and reported that the using of segmented piezoelectric sensor/actuator patches in specific positions could achieve higher control effects, less power and lighter in weight than a structure with full coverage of piezoelectric layer [8]. Meirovitch reported that misallocated

sensors and actuators might cause problems such as a lack of observability, controllability and spillover [9]. Tzou and Fu also showed that a structure bonded with full coverage of sensors and actuators could not control some modes of vibration because of the lack of observability and controllability [10].

Intensive studies have been carried out on the importance of the placement and sizing of piezoelectric sensors and actuators to suppress vibration amplitude and minimize controller energy. Piezoelectric placement and sizing are directly determined to attenuate vibration of a single mode, while it becomes much more complicated, and optimization techniques are required for vibration control of multiple modes. Active vibration reduction was investigated for plates by optimally placed actuators collected with sensors using genetic algorithms[11]-[13] based on maximization of modal and grammian controllability, [14] based on maximization of linear quadratic regulator index, and [15] based on closed-loop control and optimal linear quadratic regulator as objective functions. Roy and Chakraborty investigated a composite shell by optimally placed of actuators collected with sensors using genetic algorithms based on maximization of controllability [16] and linear quadratic regulator[17] as objective functions. Active vibration control of large-scale structures was investigated by Gawronski [18] whose placement strategy was to select a sub-search space from the overall search space on the basis of engineering experience, technical requirements and physical constraints. The optimal number was finally determined by reducing the sub-search space step by step according to the fitness value of the required numbers of sensors or actuators. This placement methodology investigated parts of a structure to reduce computation effort.

Active vibration control was investigated for plate stiffened by beams bonded with continues piezoelectric sensor and actuator either distributed by full coverage structure or

arbitrarily located of discrete sensors and actuators [19]-[21]. Stiffened plate by beams bonded with optimally placed sensor/actuator pairs was investigated by Daraji and Hale using genetic algorithms based on minimisation of linear quadratic regulator index to locate actuators as an objective function [22], effective vibration reduction obtained for all modes of vibration required to be attenuated. Balamurugan and Narayanan studied active vibration control of composite cylindrical shell stiffened by beams bonded by a full coverage sensor/actuator pair and arbitrarily located, but full coverage is not effective in sensing and controlling all modes of vibration [21].

To the authors' best knowledge, the doubly curved shell stiffened by beams has been not properly investigated by optimally placed of discrete piezoelectric sensors and actuators. In this paper, a placement methodology, fitness and objective functions are proposed to optimise the location of number of sensors collected with actuators and control feedback gain for a flexible structure under base motion, and external force excitations with applications to both small and large-scale structures. The method was implemented for a doubly curved composite cantilever shell and a doubly curved composite shell stiffened by beams using genetic algorithms. The optimization results were validated using convergence study, ANSYS package and structural vibration reduction using optimal linear quadratic control scheme.

2. MODELLING

2.1 Finite element modelling

The composite shell, stiffener and piezoelectric are modelled based on the first-order shear deformation theory using nine nodes isoparametric shell element. The composite shell and stiffener laminates are assumed to be equivalent to a solid homogenous composite structure, and the structural mass, stiffness, damping and piezoelectric coefficients are assumed to be time-invariant and linear elastic. A doubly curved composite shell element

stiffened by beams and bonded with macro fibre composite sensor/actuator pairs is shown in Figure 1. The displacements of the shell element u, v, w are related to mid-surface element nodal displacements u_{0i}, v_{0i}, w_{0i}, θ_{xi} and θ_{yi} by the shape function $N_i(s,r)$ according to equations (1) and (2) below, where the node number $i = 1-9$. The shape function represents the element geometry and the natural coordinates s and r varying between -1 and 1.

$$\begin{aligned} u(x,y,z,t) &= u_o(x,y,t) + z\theta_x(x,y,t), \\ v(x,y,z,t) &= v_o(x,y,t) + z\theta_y(x,y,t)\,, \\ w(x,y,z,t) &= w_o\,(x,y,t) \end{aligned} \tag{1}$$

$$\begin{Bmatrix} u_o \\ v_o \\ w_o \end{Bmatrix} = \sum_{i=1}^{9} N_i(s,r) \begin{Bmatrix} u_{oi} \\ v_{oi} \\ w_{oi} \end{Bmatrix} \quad , \quad \begin{Bmatrix} \theta_x \\ \theta_y \end{Bmatrix} = \sum_{i=1}^{9} N_i(s,r) \begin{Bmatrix} \theta_{xi} \\ \theta_{yi} \end{Bmatrix} \tag{2}$$

The strains induced in the shell element as a result of bending, membrane and shear effects are described by the following equations:

$$\{\boldsymbol{\varepsilon}\} = \{\boldsymbol{\varepsilon_b}\} + \{\boldsymbol{\varepsilon_m}\} + \{\boldsymbol{\gamma}\} \tag{3}$$

$$\{\boldsymbol{\varepsilon_b}\} = \begin{Bmatrix} z\dfrac{\partial \theta_x}{\partial x} \\ z\dfrac{\partial \theta_y}{\partial y} \\ z\dfrac{\partial \theta_x}{\partial y} + z\dfrac{\partial \theta_y}{\partial x} - \dfrac{z\partial u_o}{R_x \partial y} - \dfrac{z\partial v_o}{R_y \partial x} \end{Bmatrix} = \sum_{i=1}^{9} \boldsymbol{B}_{bi}\boldsymbol{\delta}_i = \boldsymbol{B}_b\boldsymbol{\delta} \tag{4}$$

$$\boldsymbol{B}_{bi} = \begin{bmatrix} 0 & 0 & 0 & z\partial N_i/\partial x & 0 \\ 0 & 0 & 0 & 0 & z\partial N_i/\partial y \\ -z\partial N_i/R_x\partial y & -z\partial N_i/R_y\partial x & 0 & z\partial N_i/\partial y & z\partial N_i/\partial x \end{bmatrix} \tag{5}$$

$$\{\boldsymbol{\varepsilon}_m\} = \begin{Bmatrix} \dfrac{\partial u_o}{\partial x} + \dfrac{w}{R_x} \\ \dfrac{\partial v_o}{\partial y} + \dfrac{w}{R_y} \\ \dfrac{\partial u_o}{\partial y} + \dfrac{\partial v_o}{\partial x} + \dfrac{2w}{R_{xy}} \end{Bmatrix} = \sum_{i=1}^{9} \boldsymbol{B}_{mi}\boldsymbol{\delta}_i = \boldsymbol{B}_m\boldsymbol{\delta} \tag{6}$$

$$\boldsymbol{B}_{mi} = \begin{bmatrix} \partial N_i/\partial x & 0 & N_i/R_x & 0 & 0 \\ 0 & \partial N_i/\partial y & N_i/R_y & 0 & 0 \\ \partial N_i/\partial y & \partial N_i/\partial x & 2N_i/R_{xy} & 0 & 0 \end{bmatrix} \tag{7}$$

$$\{\boldsymbol{\gamma}\} = \begin{Bmatrix} \theta_x - \dfrac{\partial w}{\partial x} + \dfrac{u_o}{R_x} + \dfrac{v_o}{R_{xy}} \\ \theta_y - \dfrac{\partial w}{\partial y} + \dfrac{u_o}{R_{xy}} + \dfrac{v_o}{R_y} \end{Bmatrix} = \sum_{i=1}^{9} \boldsymbol{B}_{shi}\boldsymbol{\delta}_i = \boldsymbol{B}_{sh}\boldsymbol{\delta} \tag{8}$$

$$\boldsymbol{B}_{shi} = \begin{bmatrix} N_i/R_x & N_i/R_{xy} & -\partial N_i/\partial x & N_i & 0 \\ N_i/R_{xy} & N_i/R_y & -\partial N_i/\partial y & 0 & N_i \end{bmatrix} \tag{9}$$

$$\boldsymbol{\delta} = \{\boldsymbol{\delta}_1 \quad \boldsymbol{\delta}_2 \quad \ldots. \quad \boldsymbol{\delta}_9\}^{\mathrm{T}} \ , \ \boldsymbol{\delta}_i = \{u_{oi} \quad v_{oi} \quad w_{oi} \quad \theta_{xi} \quad \theta_{yi}\}^{\mathrm{T}} \tag{10}$$

Here $\boldsymbol{B}_b$, $\boldsymbol{B}_m$ and $\boldsymbol{B}_{sh}$ are bending, membrane and shear differential matrices that relate element strains to element nodal displacements.

2.2 Piezoelectric constitutive equation

Piezoelectric materials produce electric voltage when subjected to mechanical strain and vice versa. It is a smart, light weight, large bandwidth and essential part in a control system for sensing and actuating vibration in smart structures. However, monolithic piezoceramic (PZT) imposes certain restrictions for its practical use in real-world applications. Piezoceramic is a brittle material and requires extra attention during the handling and bonding procedures. Furthermore, the adaptability to the curved surface is extremely poor requiring extra treatment of the surfaces and additional manufacturing capabilities. These restrictions are solved by using a composite monolithic piezoelectric layer in manufacturing of a developed transducer called macro fibre composite sensor and actuator (MFC). Since MFC sensors and actuators are more flexible and adaptable to the curved surface than monolith piezoceramic, they are used in this study. The linear constitutive equations of piezoelectric materials relate stresses, $\boldsymbol{\sigma}$, and electric displacement, $\boldsymbol{D}_e$ to the strains, $\boldsymbol{\varepsilon}$, and electric field, $\boldsymbol{E}_f$, vectors according to equation (11).

$$\begin{Bmatrix} \boldsymbol{\sigma} \\ \boldsymbol{D_e} \end{Bmatrix} = \begin{bmatrix} \boldsymbol{C}^{\mathrm{E}} & -\boldsymbol{e}^{\mathrm{T}} \\ \boldsymbol{e} & \boldsymbol{\mu}^{\sigma} \end{bmatrix} \begin{Bmatrix} \boldsymbol{\varepsilon} \\ \boldsymbol{E}_f \end{Bmatrix} \tag{11}$$

where $\boldsymbol{C}$, $\boldsymbol{e}$, and $\boldsymbol{\mu}$ are elasticity, piezoelectric and permittivity matrices. Superscripts *E* and σ denote that the measurements are taken under constant electrical displacement and stress, respectively.

2.3 Hamilton's principle

Hamilton's principle is used to model the stiffened shell element bonded with sensor/actuator pairs, and is as below[2]:

$$\int_{\mathrm{t1}}^{\mathrm{t2}} (\Delta \mathrm{T} - \Delta \mathrm{U} + \Delta \mathrm{W}) \mathrm{dt} = 0 \tag{12}$$

where T, U and W are the time-dependent kinetic energy, strain energy including piezoelectric energy and external applied work. The kinetic energy induced in the shell, sensor and stiffener is:

$$T = 0.5\rho \int (\dot{u}_o^2 + \dot{v}_o^2 + \dot{w}_o^2 + z^2\dot{\theta}_x^2 + z^2\dot{\theta}_y^2) dv = 0.5\dot{\boldsymbol{\delta}}^{\mathrm{T}} \boldsymbol{m} \dot{\boldsymbol{\delta}} \tag{13}$$

$$or \qquad T = 0.5\dot{\boldsymbol{\delta}}^{\mathrm{T}} \left[\boldsymbol{m}_{sl} + \boldsymbol{m}_{pz} + \boldsymbol{m}_{st}\right] \dot{\boldsymbol{\delta}} = 0.5\dot{\boldsymbol{\delta}}^{\mathrm{T}} \boldsymbol{M} \dot{\boldsymbol{\delta}} \tag{14}$$

where subscripts sl , pz and st refer to shell, piezoelectric and stiffener, respectively. The total strain energy U induced in a shell with stiffeners and piezoelectric sensors, including the electrical energy, can be described by the following equation:

$$U = \frac{1}{2} \int_v \boldsymbol{\varepsilon}^{\mathrm{T}} \boldsymbol{\sigma} \, dv - \frac{1}{2} \int_v \boldsymbol{E}_f{}^{\mathrm{T}} \boldsymbol{D}_e dv \tag{15}$$

The distribution of the electrical field, $\boldsymbol{E}_f$, in the z-direction, E_z, varies linearly across the thickness of a piezoelectric element h_{pz} , and the voltage difference across its thickness is constant over its whole area. Hence,

$$E_z = \frac{\Delta\phi}{h} \quad , \quad \boldsymbol{E}_f = \begin{Bmatrix} 0 \\ 0 \\ 1/h_{pz} \end{Bmatrix} \phi = \boldsymbol{B}_{\emptyset}\phi \tag{16}$$

where ϕ has a single voltage degree of freedom induced over the top centre surface of the piezoelectric.

$$U = 0.5\boldsymbol{\delta}^T \int_v \{(\boldsymbol{B}_b^{\mathrm{T}}\boldsymbol{D}\boldsymbol{B}_b + \boldsymbol{B}_m^{\mathrm{T}}\boldsymbol{D}\boldsymbol{B}_m + \boldsymbol{B}_m^{\mathrm{T}}\boldsymbol{D}\boldsymbol{B}_b + \boldsymbol{B}_b^{\mathrm{T}}\boldsymbol{D}\boldsymbol{B}_m + \boldsymbol{B}_{sh}^{\mathrm{T}}\boldsymbol{G}\boldsymbol{B}_{sh} + \boldsymbol{B}_{\emptyset}^{\mathrm{T}}\boldsymbol{e}\boldsymbol{B}_b + \boldsymbol{B}_{\emptyset}^{\mathrm{T}}\boldsymbol{e}\boldsymbol{B}_m)\boldsymbol{\delta} - (\boldsymbol{B}_b^{\mathrm{T}}\boldsymbol{e}^{\mathrm{T}}\boldsymbol{B}_{\emptyset} + \boldsymbol{B}_m^{\mathrm{T}}\boldsymbol{e}^{\mathrm{T}}\boldsymbol{B}_{\emptyset} - \boldsymbol{B}_{\emptyset}^{\mathrm{T}}\boldsymbol{\mu}\boldsymbol{B}_{\emptyset})\boldsymbol{\phi}\}dv \tag{17}$$

$$U = 0.5(\boldsymbol{\delta}^{\mathrm{T}}\boldsymbol{K}\boldsymbol{\delta} - \boldsymbol{\delta}^{\mathrm{T}}\boldsymbol{K}_{u\emptyset}^{s}\boldsymbol{\phi} - \boldsymbol{\phi}^{\mathrm{T}}\boldsymbol{K}_{\emptyset u}^{s}\boldsymbol{\delta} - \boldsymbol{\phi}^{\mathrm{T}}\boldsymbol{K}_{\emptyset\emptyset}^{s}\boldsymbol{\phi} - \boldsymbol{\delta}^{\mathrm{T}}\boldsymbol{K}_{u\emptyset}^{a}\boldsymbol{\phi} - \boldsymbol{\phi}^{\mathrm{T}}\boldsymbol{K}_{\emptyset u}^{a}\boldsymbol{\delta} - \boldsymbol{\phi}^{\mathrm{T}}\boldsymbol{K}_{\emptyset\emptyset}^{a}\boldsymbol{\phi}) \tag{18}$$

The work done by the mechanical and electric forces is given by:

$$\Delta W = \Delta\boldsymbol{\delta}^{\mathrm{T}}\boldsymbol{F}_{\boldsymbol{u}} + \Delta\boldsymbol{\delta}^{\mathrm{T}}\boldsymbol{M}\boldsymbol{I}\ddot{\boldsymbol{r}} - \Delta\boldsymbol{\phi}^{\mathrm{T}}\boldsymbol{F}_{\phi} \tag{19}$$

where $\boldsymbol{F}_u$, $\boldsymbol{F}_{\phi}$ and $\ddot{\boldsymbol{r}}$ refer to mechanical force, piezoelectric charge and base motion excitation, respectively. By substituting equations (14), (18) and (19) into equation (12) the following equations are obtained:

$$\int_{t1}^{t2} (-\Delta\boldsymbol{\delta}^{\mathrm{T}}\boldsymbol{M}\ddot{\boldsymbol{\delta}} - \Delta\boldsymbol{\delta}^{\mathrm{T}}\boldsymbol{K}\boldsymbol{\delta} + \Delta\boldsymbol{\delta}^{\mathrm{T}}\boldsymbol{K}_{u\emptyset}\boldsymbol{\phi} + \Delta\boldsymbol{\phi}^{\mathrm{T}}\boldsymbol{K}_{\emptyset u}\boldsymbol{\delta} + \Delta\boldsymbol{\phi}^{\mathrm{T}}\boldsymbol{K}_{\emptyset\emptyset}\boldsymbol{\phi} + \Delta\boldsymbol{\delta}^{\mathrm{T}}\boldsymbol{F}_{\boldsymbol{u}} + \Delta\boldsymbol{\delta}^{\mathrm{T}}\boldsymbol{M}\boldsymbol{I}\ddot{\boldsymbol{r}} - \Delta\boldsymbol{\phi}^{\mathrm{T}}\boldsymbol{F}_{\phi})\mathrm{dt} = 0 \tag{20}$$

$$\boldsymbol{M}\ddot{\boldsymbol{\delta}} + \boldsymbol{K}\boldsymbol{\delta} = \boldsymbol{F}_{\boldsymbol{u}} + \boldsymbol{M}\boldsymbol{I}\ddot{\boldsymbol{r}} - \boldsymbol{K}_{u\emptyset}^{a}\boldsymbol{\phi}_a \tag{21}$$

$$\boldsymbol{K}_{\emptyset u}^{a}\boldsymbol{\delta} + \boldsymbol{K}_{\emptyset\emptyset}^{a}\,\boldsymbol{\phi}_a = \boldsymbol{F}_{\phi} \tag{22}$$

$$\boldsymbol{K}_{\emptyset u}^{s}\boldsymbol{\delta} + \boldsymbol{K}_{\emptyset\emptyset}^{s}\boldsymbol{\phi}_s = 0 \tag{23}$$

Equations (21), (22) and (23) represent the dynamic equilibrium equations for a stiffened shell bonded with piezoelectric sensors and actuators. Equation (21) could be improved by adding the structural damping force $\boldsymbol{C}_{\boldsymbol{d}}\dot{\boldsymbol{\delta}}$ as follows:

$$\boldsymbol{M}\ddot{\boldsymbol{\delta}} + \boldsymbol{C}_{\boldsymbol{d}}\dot{\boldsymbol{\delta}} + \boldsymbol{K}\boldsymbol{\delta} = \boldsymbol{F}_{\boldsymbol{u}} + \boldsymbol{M}\boldsymbol{I}\ddot{\boldsymbol{r}} - \boldsymbol{K}_{u\emptyset}^{a}\boldsymbol{\phi}_a \tag{21}$$

2.4 Modal coordinate

Conversion of the above dynamic equations from physical to modal coordinates decouples the equation system so that each mode can be investigated individually and the computational cost can be significantly reduced. The relationships between the physical and modal displacements are represented by the following equations:

$$\boldsymbol{\delta} = \boldsymbol{\varphi}\,\boldsymbol{\eta} \quad , \quad \dot{\boldsymbol{\delta}} = \boldsymbol{\varphi}\,\dot{\boldsymbol{\eta}} \quad , \quad \ddot{\boldsymbol{\delta}} = \boldsymbol{\varphi}\,\ddot{\boldsymbol{\eta}} \tag{24}$$

$$\boldsymbol{\varphi}^{\mathrm{T}}\boldsymbol{M}\boldsymbol{\varphi} = \boldsymbol{I} \quad , \quad \boldsymbol{\varphi}^{\mathrm{T}}\boldsymbol{K}\boldsymbol{\varphi} = \boldsymbol{\Omega}\,, \quad \boldsymbol{\varphi}^{\mathrm{T}}\boldsymbol{C_d}\boldsymbol{\varphi} = 2\boldsymbol{\xi}\boldsymbol{\omega} \tag{25}$$

where $\boldsymbol{\varphi}$ is an open-loop mass-normalised modal matrix obtained by solving the undamped eigenvalue problem and $\boldsymbol{\eta}$ is a single vector of the modal coordinates. The mass, stiffness, structural damping factor and damping ratio of the system are denoted by $\boldsymbol{M}, \boldsymbol{K}, \boldsymbol{C_d}$ and $\boldsymbol{\xi}$, respectively. By substituting equations (24) and (25) into equations (21) and (23), the following equations are obtained after adding structural damping:

$$\ddot{\boldsymbol{\eta}} + 2\boldsymbol{\xi}\boldsymbol{\omega}\dot{\boldsymbol{\eta}} + \boldsymbol{\omega^2}\,\boldsymbol{\eta} = \boldsymbol{\varphi}^{\mathrm{T}}\boldsymbol{F_u} + \boldsymbol{\varphi}^{\mathrm{T}}\boldsymbol{M}\boldsymbol{I}\ddot{\boldsymbol{r}} - \boldsymbol{\varphi}^{\mathrm{T}}\boldsymbol{K}^{a}_{u\emptyset}\boldsymbol{\phi}_a \tag{26}$$

$$\boldsymbol{\phi}_s = -\boldsymbol{\varphi}^{\mathrm{T}}{\boldsymbol{K}^{s}_{\emptyset\emptyset}}^{-1}\boldsymbol{K}^{s}_{\emptyset u}\boldsymbol{\eta} \tag{27}$$

Introducing the state variables $\boldsymbol{X}$ and $\dot{\boldsymbol{X}}$ below into equations (26) and (27) yields the following state space equations:

$$\boldsymbol{X} = \begin{Bmatrix}\boldsymbol{X}_1\\ \boldsymbol{X}_2\end{Bmatrix} = \begin{Bmatrix}\boldsymbol{\eta}\\ \dot{\boldsymbol{\eta}}\end{Bmatrix} \quad , \quad \dot{\boldsymbol{X}} = \begin{Bmatrix}\dot{\boldsymbol{X}}_1\\ \dot{\boldsymbol{X}}_2\end{Bmatrix} = \begin{Bmatrix}\dot{\boldsymbol{\eta}}\\ \ddot{\boldsymbol{\eta}}\end{Bmatrix} \tag{28}$$

$$\dot{\boldsymbol{X}} = \begin{bmatrix}0 & \omega\\ -\omega & -2\xi\omega\end{bmatrix}\boldsymbol{X} + \begin{bmatrix}0\\ -\boldsymbol{\varphi}^{\mathrm{T}}\boldsymbol{K}^{a}_{u\emptyset}\end{bmatrix}\boldsymbol{\phi}_a + \begin{bmatrix}0\\ \boldsymbol{\varphi}^{\mathrm{T}}\end{bmatrix}\boldsymbol{F}_u + \begin{bmatrix}0\\ -\boldsymbol{\varphi}^{T}\boldsymbol{M}\boldsymbol{\omega^2}\boldsymbol{I}\end{bmatrix}\boldsymbol{r} \tag{29}$$

$$\dot{\boldsymbol{X}} = \boldsymbol{A}\boldsymbol{X} + \boldsymbol{B_1}\boldsymbol{\phi}_a + \boldsymbol{B_2}\boldsymbol{F}_d + \boldsymbol{B_3}\boldsymbol{r} \quad , \quad \boldsymbol{\phi}_s = \boldsymbol{C}\,\boldsymbol{X} \tag{30}$$

$$\boldsymbol{A}_i = \begin{bmatrix}0 & \omega_i\\ -\omega_i & -2\xi_i\omega_i\end{bmatrix} \quad , \quad \boldsymbol{B}1_i = \begin{bmatrix}0\\ -\boldsymbol{\varphi}^{\mathrm{T}}\boldsymbol{K}^{a}_{u\emptyset}\end{bmatrix} \tag{31}$$

$$\boldsymbol{B}2_{\boldsymbol{i}} = \begin{bmatrix}0\\ \boldsymbol{\varphi}^{\mathrm{T}}\end{bmatrix} \quad , \quad \boldsymbol{B}3_{\boldsymbol{i}} = \begin{bmatrix}0\\ -\boldsymbol{\varphi}^{\mathrm{T}}\boldsymbol{M}\boldsymbol{\omega^2}\boldsymbol{I}\end{bmatrix} \tag{32}$$

$$\boldsymbol{C_i} = \left[-\boldsymbol{\varphi}^{\mathrm{T}}\boldsymbol{\omega_i^{-1}}\,\boldsymbol{K_{\emptyset\emptyset}^{s}}^{-1}\boldsymbol{K_{u\emptyset}^{s}} \quad 0\right] \quad , \qquad \boldsymbol{X}_i = \{\omega_i\eta_i \quad \dot{\eta}_i\}^{\mathrm{T}} \tag{33}$$

where $\boldsymbol{A}_i$, $\boldsymbol{B}1_i$, $\boldsymbol{B}2_i$, $\boldsymbol{B}3_i$, $\boldsymbol{C}_i$ and $\boldsymbol{X}_i$ are individual modal state, input actuator, external mechanical force excitation, external base motion excitation, output sensor matrices and state vector, respectively. The state, sensor and actuator matrices for n_m modes and r_a sensor and actuator patches are given by:

$$\boldsymbol{A}_{(2n_m\times 2n_m)} = \begin{bmatrix} \boldsymbol{A}_1 & \cdots & 0 \\ \vdots & \ddots & \vdots \\ 0 & \cdots & \boldsymbol{A}_{n_m} \end{bmatrix} \tag{34}$$

$$\boldsymbol{B}1_{(2n_m\times r_a)} = \begin{bmatrix} (\boldsymbol{B}_1)_1 & \cdots & (\boldsymbol{B}_1)_{r_a} \\ \vdots & \cdots & \vdots \\ (\boldsymbol{B}_1)_{nm} & \cdots & (\boldsymbol{B}_1)_{r_a} \end{bmatrix} \tag{35}$$

$$\boldsymbol{C}_{(r_a\times 2n_m)} = \begin{bmatrix} (\boldsymbol{C})_1 & \cdots & (\boldsymbol{C})_{nm} \\ \vdots & \cdots & \vdots \\ (\boldsymbol{C})_{r_a} & \cdots & (\boldsymbol{C})_{r_a} \end{bmatrix} \tag{36}$$

$$\boldsymbol{X}_{(2n_m\times 1)} = \{\omega_1\eta_1 \quad \dot{\eta}_1 \quad \cdots \quad \omega_{n_m}\eta_{n_m} \quad \dot{\eta}_{n_m}\}^T \tag{37}$$

3. CONTROL SCHEME

Optimal linear quadratic control scheme was used to attenuate structural vibration. The determination of optimal feedback control gain was based on the minimisation of the performance index *J*:

$$J = \int_0^\infty (\boldsymbol{X}^T\boldsymbol{Q}\boldsymbol{X} + \boldsymbol{\phi}_a^T\boldsymbol{R}\boldsymbol{\phi}_a)dt \tag{38}$$

The matrices $\boldsymbol{Q}$ of dimensions $2n_m \times 2n_m$ and $\boldsymbol{R}$ of dimensions $r_a \times r_a$ are diagonal, positive definite and real symmetrical matrices. Matrix $\boldsymbol{Q}$ is directly proportional to the vibration reduction and external controller energy. The minimisation of optimal linear quadratic index leads to the following Riccati equation:

$$\boldsymbol{A}^T\boldsymbol{P} + \boldsymbol{P}\boldsymbol{A} - \boldsymbol{P}\boldsymbol{B}\boldsymbol{R}^{-1}\boldsymbol{B}^T\boldsymbol{P} + \boldsymbol{Q} = 0 \tag{39}$$

$$\boldsymbol{K} = \boldsymbol{R}^{-1}\boldsymbol{B}^T\boldsymbol{P}\,, \qquad \boldsymbol{\phi}_a = -\boldsymbol{K}\boldsymbol{X} \tag{40}$$

The matrices $\boldsymbol{A}$, $\boldsymbol{B}$, $\boldsymbol{C}$, and $\boldsymbol{K}$ refer to the structure state space, piezoelectric actuators, sensors matrices determined by equations (34-36), and control gain matrices shown in the Simulink Figure 2.

For a given control system, all the parameters of the Reduced Riccati equation (39) are known, from which matrix $\boldsymbol{P}$ can be solved. The control system is stable or the closed loop control is stable if the trace of matrix $\boldsymbol{P}$ is positive definite. Controller gain is obtained after substitution of matrix $\boldsymbol{P}$ in equation (40). In this study, the optimal actuator matrix $\boldsymbol{B}$ was determined by pairing actuators with optimal sensor locations to get optimal controller feedback gain $\boldsymbol{K}$ and actuator feedback voltage $\boldsymbol{\phi}_a$ from equation (40). The Simulink diagram shown in Figure 2 is based on the optimal linear quadratic control scheme to test the effectiveness of the optimal locations of the sensor/actuator pairs for the stiffened shell.

In this study, the actuators were located in paired with optimal sensors locations to prevent the effect of spillover phenomena at the dominant structure frequencies, however in real life application, the spillover phenomena and delay due actuator time constant arises during excitation of higher modes.

4. OBJECTIVE FUNCTION

In this study, an objective function is developed for optimal placement of sensor/actuator pairs based on the maximisation of sensor output voltage for a structure subjected to either motion base excitation or external force excitation. Consider the state space equation (30), which describes the dynamic motion of a structure under external actuator voltage $\boldsymbol{\phi}_a$, force $\boldsymbol{F}_u$ and base motion $\boldsymbol{r}$ excitations:

$$\dot{\boldsymbol{X}} = \boldsymbol{AX} + \boldsymbol{B_1\phi}_a + \boldsymbol{B_2F}_d + \boldsymbol{B_3r} \tag{41}$$

Firstly, the optimal sensor placement is investigated for a structure under base motion excitation $\boldsymbol{r}$ to find the optimal sensor location. Taking the Laplace transforms of both sides of equation (41), after eliminating the effects of the external actuator excitation voltage $\boldsymbol{\phi}_a$ and the external excitation force $\boldsymbol{F}_u$, yields:

$$\boldsymbol{sX}(s) = \boldsymbol{AX}(s) + \boldsymbol{B_3 r}(s) \tag{42}$$

$$\boldsymbol{X}(s) = \boldsymbol{B_3 r}(s)\ (\boldsymbol{s} - \boldsymbol{A})^{-1} \tag{43}$$

$$\boldsymbol{\phi}_s = \boldsymbol{CX} \tag{44}$$

Taking the Laplace transform of equation (44) results in:

$$\boldsymbol{\phi}_s(s) = \boldsymbol{CX}(s) \tag{45}$$

From equations (45) and (42):

$$\boldsymbol{\phi}_s(s) = \boldsymbol{C}\ (\boldsymbol{s} - \boldsymbol{A})^{-1}\ \boldsymbol{B_3 r}(s) \tag{46}$$

The output sensor voltage in the frequency domain at a single mode of vibration is:

$$\boldsymbol{\phi}_s = \boldsymbol{C}(j\boldsymbol{\omega I} - \boldsymbol{A})^{-1}\boldsymbol{B_3 r} \tag{47}$$

The output voltage of sensor n_s as a results of applying external base motion excitation $\boldsymbol{r}$ at multiple modes of vibration m_n is:

$$\boldsymbol{\phi}_s(n_s, n_m) = \boldsymbol{C}(j\boldsymbol{\omega I} - \boldsymbol{A})^{-1}\boldsymbol{B_3}\ \boldsymbol{r} \tag{48}$$

Secondly, the optimal sensor placement is considered for the structure under external force excitation, in the same way, the sensor voltage calculated as a results of applying external force excitation at multiple modes of vibration m_n is:

$$\boldsymbol{\phi}_s(n_s, n_m) = \boldsymbol{C}(j\boldsymbol{\omega I} - \boldsymbol{A})^{-1}\boldsymbol{B_2 F}_u \tag{49}$$

The total voltage $V_s(x, y)$ of the sensors under multiple modes of vibration are the fitness function, i.e.,

$$V_s(x, y) = \sum_{j=1}^{n_m} \sum_{i=1}^{n_s} \boldsymbol{\phi}_s(i, j) \tag{50}$$

$$J(x, y) = \max(V_s(x, y)), 1/\boldsymbol{K}(x, y)) \tag{51}$$

Equation (51) represents an objective function under the condition of x and $y \in$ structural dimensions to find the optimal sensor location. The optimal feedback gain $\boldsymbol{K}(x, y)$ is determined based on the equations (39) and (40) after finding the optimal sensor locations.

5. PLACEMENT METHODOLOGY USING GENETIC ALGORITHMS

Genetic algorithm is a superior guided random method based on the principle of survival of the fittest or natural evolution theory, which is invented by Holland in 1975. It has been continuously improved and become a powerful method for searching optimal solutions. The search space in an optimisation problem normally consists of a large number of candidate solutions directly proportional to the number of, e.g., optimised piezoelectric elements and number of possible locations on a structure. Population individuals are the fundamental unit of genetic algorithms, each of which is defined by chromosome containing a number of genes. Each of these individuals is marked by a fitness value depending on definition of fitness function for the optimisation problem and the optimal solution is the fittest one. The members of the populations with the highest fitness values are allowed to breed to form the next generation, and the process continues until convergence is achieved. The chromosome contains a number of genes coded by integer numbers, each of which represents a sensor or an actuator with its location properties. The string length of a chromosome is equal to the number of sensors or actuators required to be optimised.

In this study, an optimisation placement methodology was developed and programmed using MATLAB m-code to determine optimal locations of a given number of discrete piezoelectric sensor/actuator pairs. There are the following main steps.

1. Use a finite element model to determine the mass normalised free vibration mode shapes and the associated natural frequencies for a selected number,n_m, of modes of vibration.

2. Formulate the state space matrix $\boldsymbol{A}$ of dimension $(2n_m, 2n_m)$ for the selected number of modes of vibration (see equation 34).
3. Formulate excitation matrices $\boldsymbol{B}2$ for external force excitation, or $\boldsymbol{B}3$ for base motion excitation to drive the structure at the resonance modes (see equation 32).
4. Choose a suitably large number of chromosomes randomly from the search space to form the initial population.
5. Calculate the output sensor matrix $\boldsymbol{C}$ for each chromosome and for the n_m modes of vibration (see equation 36).
6. Calculate the fitness value for each member of the population based on the fitness function (see equation 50).
7. Rank the chromosomes by their fitness values and select the largest fitness chromosomes to form the breeding population. The selected are called parents, and the remaining less fit chromosomes are discarded (see equation 51).
8. Pair up the members of the breeding populations in the order of fitness and apply a selected percentage crossover to each pair. The crossover points are selected randomly and are different for each parents. This gives two new offspring (child) chromosomes with new properties.
9. Apply a small percentage mutation rate to the child chromosomes.
10. Identify any repeated genes from the new chromosomes. Any detected is replaced with a gene from the search space.
11. Calculate the output sensor matrix $\boldsymbol{C}$ for each child chromosome.
12. Repeat the steps from step 7 for a required number of generations.

6. RESULTS AND DISCUSSION

The proposed sensor placement methodology using genetic algorithms is applied in this Section to find the optimal placement of four sensor/actuator pairs for both doubly curved composite shell and the doubly curved composite shell stiffened by four curved beams located symmetrically as shown in Figures 3 and 4. These optimisation problems create search spaces of 3.92×10^6 candidate solutions for the cantilever shell and 1.04×10^8 candidate solutions for the stiffened shell, while only one candidate solutions is the global optimal

solution for each case. The composite cantilever shell and stiffened composite shell are made of laminated carbon fibre composites (T300/5208) with a section profile of $[0_4/45_4/90_4]$.

6.1 Research problem description

6.1.1 Doubly curved composite shell

The cantilever composite shell shown in Figure 3 represents an optimisation problem of moderate complexity. The shell dimensions are 500×500×3 mm with radii of curvature 1500 mm. The shell surface was discretised into one hundred sub-areas representing 10×10 locations, as shown in Figure 3, where piezoelectric sensor segment of 40×40×0.3 mm were bonded. Table 1 shows the properties of the shell and the piezoelectric sensors. The smart shell was subjected to external sinusoidal force excitation at structural natural frequencies to excite structure resonance. The proposed placement methodology explained in Sections 4 and 5 were applied to get the optimal distribution of four sensor/actuator pairs and feedback gain based on the maximization of sensor output voltages and minimisation of optimal linear quadratic index. The importance of this placement methodology based on the external excitation force is more effective than other methodologies in the literatures when the location of the external excitation vibration force is known.

6.1.2 Doubly curved stiffened composite shell

The stiffened composite shell represents an optimisation problem of larger-scale structure and significant complexity. The stiffened shell has dimensions of 1500×1500×3 mm with radii of curvature 6500 mm and is stiffened by four curved beams located symmetrically as shown in Figure 4. The surface of the shell was discretised into 225 sub-areas representing 15×15 individual locations. The stiffened shell was mounted rigidly along all the edges and subjected to base motion excitation of sinusoidal displacement at all mounted edges in the z-direction. Optimal placement of four macro fibre composite sensor/actuator pairs and feedback gain

was optimised using the proposed methodology, and the genetic algorithms explained in Sections 4 and 5.

6.2 Natural frequency

The doubly curved composite shell and the stiffened composite shell are modelled by ANSYS package to determine the first six natural frequencies. Table 2 shows the first six natural frequencies of the two composite shells with and without sensors in the optimal locations. Adding the mass and the stiffness of the macro fibre composite sensors to the main structure reduces and increases the natural frequencies, respectively. The results of natural frequencies for both shells shown in Table 2 are all slightly increased. Thus increasing in natural frequencies demonstrates the effect of the sensor stiffness on the natural frequencies is larger than mass effect.

6.3 Optimal placement for a cantilever shell

The optimal placement of four sensor/actuator pairs and feedback gain is investigated for the unstiffened shell using the genetic algorithms placement methodology explained in Sections 4 and 5. The shell is subjected to a sinusoidal external excitation force of 2.0 N at the free end. In this study, a Matlab m-file program is written based on the modelling and placement methodology to find the optimal sensor/actuator locations. Figure 5 shows three steps of the progressive convergence of the population around the circle with radius r which represents the fitness value to be maximized. The first generation of the population is very close to the centre with representative of high and low fitness and a range in between. After ten generations, the population is much less diverse and have moved away from the centre, made up of individuals of high, though not yet optimised fitness. After 50 generations the

population has converted to a level of fitness higher than any individual in the first or ten generations.

The convergence to the optimal solution is shown in another form in Figure 6. Each point represents a location of s/a pairs for one of individual of a particular generation. In the first generation, these locations are widely spread, having been selected at random. After 10 generations, they have begun to cluster in a few locations, and after 50 generations the clustering is completed with all individual chromosomes coding for sensors at the four most efficient locations distributed at the root of the cantilever shell.

The genetic algorithms program was repeatedly run to test the effectiveness of the placement methodology and repeatability of the optimised s/a locations. The results shown in Figure 7 give an indication of the progress of each run by plotting the fitness of the fittest member of the breeding population at each generation. It can be seen that the final fitness value is almost the same, though the path by which it is reached is different for each run. This indicates that the process is robust in finding the optimal solution repeatedly and is a powerful method to find the global optimal solution for a complex optimisation problem.

The procedure is further applied to optimise the locations of four sensor/actuator pairs for the stiffened composite shell mounted rigidly along its four side edges. The shell is subjected to sinusoidal base motion excitation of 1mm amplitude. Again, the first six natural frequencies are considered. The progression results of the optimal placement are shown in Figures 8-10.

6.4 Results validation

To validate the optimal s/a locations and the importance of discrete s/a pairs, two stiffened composite shells are considered. The first stiffened composite shell is bonded with

a full coverage of a single sensor layer of dimension 1500×1500×0.3 mm and the second stiffened shell is bonded with 225 discrete sensors of dimension 90×90×0.3 mm each. Both stiffened shells are mounted rigidly from all edges and subjected to base sinusoidal motion excitation of 1 mm amplitude at shell's natural frequencies. Both shells are modelled by ANSYS to investigate the distribution of the voltage generated by the sensors and to validate the optimal locations of the sensor/actuator pairs obtained in the previous Section using the genetic algorithm, and to investigate the importance of locating sensors and actuators optimally compared to the full coverage of single s/a pairs for stiffened structures investigated in the literature.

Figures 11 and 12 shows ANSYS result of the electric field distribution and sensor voltage generation when the stiffened shell bonded with a full coverage of a single sensor layer is forced to vibrate at its first and third natural frequencies. It can be observed from Figure 11 that the electric field is distributed symmetrically about the horizontal axis and anti-symmetrically about the vertical axis. This distribution agrees with the results of the optimal four sensors locations obtained in the previous Section using the genetic algorithms (Figure 9). The anti-symmetric distribution of the electric field results in cancellation of any voltage generated by the sensor, thus a total output voltage close to zero as shown in Figure 12. The voltage cancellation was also observed for the forced vibration at other natural frequencies. Figures 11 and 12 approve that there is no sensing and actuating for a composite shell stiffened by beams bonded with full coverage of single s/a pair.

Figure 13 shows sensors voltage distribution ranging between the high and low voltage at the first and third modes of vibration for the composite shell stiffened by beams bonded with full coverage of 225 discrete independent sensors. The figure also shows that the location of maximum sensor voltage distribution agrees well with the optimal four sensor locations

obtained at the previous Section using genetic algorithms (Figure 9). It can be observed from Figure 13 that the sensors voltage is much higher (2.18 V for sensor size 90×90 mm) than the voltage generated by a single sensor (0.031 V for sensor size 1500×1500 mm) shown in Figure 12. The study in this Section exhibits the important of using discrete sensors and actuators at optimally location for active vibration control.

6.5 Active vibration reduction

Stiffened composite shells bonded with optimally placed and non-optimised four s/a pairs are investigated as shown in Figure (14). A sinusoidal excitation voltage of $100\sin\omega_i t$ was applied on the actuator located at the position 05 for both case study shown in Figure (14), to actuate the stiffened shell at the 1st, 2nd, 3rd, 4th, 5th and 6th modes, respectively. A Matlab m-file and a Simulink model for active vibration reduction were designed based on the model explained in Sections 3 and 4 using optimal linear quadratic control. The controller weighting matrices are diagonal and manually tuned by setting R to unity and increasing Q matrix gradually to get an effective vibration attenuation with low feedback voltage which found at Q equal 10^8. The optimisation of vibration reduction at low feedback voltage and high response were achieved based optimal location of piezoelectric sensors and actuators.

A comparison of sensor voltage generation based on vibration detection was made for the two cases study under the same sinusoidal voltage excitation applied on actuator location 05. Table 3 shows the output sensor voltage for the optimised and non-optimised sensor location. It can be shown from Table 3 that the output sensor voltage for the optimised case is much higher than non-optimised case for the same excitation voltage. The lower sensors voltage demonstrates that the non-optimised case is unobservable and uncontrollable at

most modes of vibration. This results highlighted the important of discrete sensor, actuator and their locations than non-optimised and full coverage of single sensor/actuator pair.

Active vibration reduction of the above stiffened composite shells bonded with optimally placed four sensor/actuator pairs (case1) is studied using the optimal linear quadratic control scheme. Figures (15-17) show the results of the transient and steady state time responses of the open loop sensor voltage (OLSV), closed loop sensor voltage (CLSV), actuator feedback voltage (CLAV) and external disturbance excitation voltage (EV) of $100\sin \omega_i t$ at the first, third and fifth natural modes of vibration, respectively.

A large percentage vibration reduction was found by comparing the CLSV with the OLSV and a reduction up to 96.6%, 95%, 99.3%, 98.8%, 97.5% and 99% can be achieved, respectively, at the first six modes. These results demonstrate the effectiveness of the optimal sensor/actuator pairs and placement method for simple and complex structures.

Figures (15-17) show a high speed response of vibration detection by sensors and attenuation by actuators at the transient response zone. It can be observed from the Figures that the vibration sensing and attenuation started at lower than 0.001 seconds after the external disturbance was applied. This indicates that the optimal locations of the sensor/actuator pairs on the stiffened composite shell determined by this study are highly effective for vibration sensing and suppression.

7. CONCLUSION

In this study, an objective function for active vibration control using genetic algorithm was developed based on generating a maximum voltage of the piezoelectric sensor bonded on a structure that vibrates under an external force or base motion excitation. The placement method is very efficient for a structure under external force excitation, and the placement

under base motion excitation could be used for a general simple and complex structures in geometry. The placement method was tested using doubly curved shells stiffened with beams and bonded with macro fibre composite sensor/actuator pairs. Optimal linear quadratic control scheme was used to find optimal feedback control gain and attenuate structural vibration.

The genetic algorithm optimal placement method was applied for a cantilever composite doubly curved shell of dimensions to optimise the locations of four sensor/actuator pairs to attenuate the first six modes of vibration; then the method was implemented for a larger composite shell stiffened by four curved beams located symmetrically. The optimal sensor/actuator pairs was found to be distributed symmetrically about the shell axis of symmetry. The optimal locations was validated by running the genetic algorithms computer program repeatedly multiple times, giving same optimal sensor locations with different routes to reach the same optimal fitness at each time. The optimal location was also tested in ANSYS package by covering the whole structure surface by a single piezoelectric sensor to find the sensor voltage distribution over the surface. The sensor voltage distribution was found to be similar to the optimal sensor locations determined in genetic algorithms. Also, the ANSYS test shows the drawback-effect of using single sensor covering the whole structure area resulting in cancellation of the sensor voltage output due to the effects of the summation of the negative and the positive voltage values.

The optimised sensor/actuator locations on the stiffened shell were tested for active vibration reduction using optimal linear quadratic control and compared with the non-optimised location. The non-optimised case was unobservable and uncontrollable since the output sensor voltage was found to be much lower than the optimised case. Large vibration

reduction was obtained within the high response and low feedback actuator voltage at steady state for the first six modes of vibration.

ACKNOWLEDGMENT

The authors at Lancaster University and Coventry University are grateful to the EPSRC for financial support (EP/K020080/1).

REFERENCES

[1] H. Allik and T. J. R. Hughes, "Finite element method for piezoelectric vibration," *Int. J. Numer. methods engineering*, vol. 2, no. 2, pp. 151–157, 1970.

[2] H. S. Tzou and C. I. Tseng, "Distributed piezoelectric sensor/actuator design for dynamic measurement/control of distributed parameter systems: A piezoelectric finite element approach," *J. Sound Vib.*, vol. 138, no. 1, pp. 17–34, 1990.

[3] D. T. Detwiler, M.-H. H. Shen, and V. B. Venkayya, "Finite element analysis of laminated composite structures containing distributed piezoelectric actuators and sensors," *Finite Elem. Anal. Des.*, vol. 20, no. 2, pp. 87–100, 1995.

[4] S. A. Kulkarni and K. M. Bajoria, "Finite element modeling of smart plates/shells using higher order shear deformation theory," *Compos. Struct.*, vol. 62, no. 1, pp. 41–50, 2003.

[5] J. N. Reddy, "On laminated composite plates with integrated sensors and actuators," *Eng. Struct.*, vol. 21, no. 7, pp. 568–593, 1999.

[6] R. Kumar, B. K. Mishra, and S. C. Jain, "Static and dynamic analysis of smart cylindrical shell," *Finite Elem. Anal. Des.*, vol. 45, no. 1, pp. 13–24, 2008.

[7] V. Balamurugan and S. Narayanan, "Shell finite element for smart piezoelectric composite plate/shell structures and its application to the study of active vibration control," *Finite Elem. Anal. Des.*, vol. 37, no. 9, pp. 713–718, 2001.

[8] Y.-H. Lim, "Finite-element simulation of closed loop vibration control of a smart plate under transient loading," *Smart Mater. Struct.*, vol. 12, no. 2, pp. 272–286, 2003.

[9] L. Meirovitch, *Dynamics and control of structures*. Canda: Wiley, 1990.

[10] J.-H. Han and I. Lee, "Optimal placement of piezoelectric sensors and actuators for vibration control of a composite plate using genetic algorithms," *Smart Mater. Struct.*, vol. 8, no. 2, pp. 257–267, 1999.

[11] A. M. Sadri, J. R. Wright, and R. J. Wynne, "Modelling and optimal placement of piezoelectric actuators in isotropic plates using genetic algorithms," *Smart Mater. Struct.*, vol. 8, no. 4, pp. 490–498, 1999.

[12] A. M. Sadri, J. R. Wright, and R. J. Wynne, "LQG control design for panel flutter suppression using piezoelectric actuators," *Smart Mater. Struct.*, vol. 11, no. 6, pp. 834–839, 2002.

[13] F. Peng, "Actuator Placement Optimization and Adaptive Vibration Control of Plate Smart Structures," *J. Intell. Mater. Syst. Struct.*, vol. 16, no. 3, pp. 263–271, 2005.

[14] K. Ramesh Kumar and S. Narayanan, "The optimal location of piezoelectric actuators and sensors for vibration control of plates," *Smart Mater. Struct.*, vol. 16, no. 6, pp. 2680–2691, 2007.

[15] A. H. Daraji and J. M. Hale, "Reduction of structural weight, costs and complexity of a control system in the active vibration reduction of flexible structures," *Smart Mater. Struct.*, vol. 23, no. 9, 2014.

[16] T. Roy and D. Chakraborty, "Optimal vibration control of smart fiber reinforced composite shell structures using improved genetic algorithm," *J. Sound Vib.*, vol. 319, no. 1–2, pp. 15–40, 2009.

[17] T. Roy and D. Chakraborty, "Genetic algorithm based optimal control of smart composite shell structures

under mechanical loading and thermal gradient," *Smart Mater. Struct.*, vol. 18, no. 11, p. 115006, 2009.

[18] W. K. Gawronski, *advance structural dynamics and active control and structures*. New York: Springer, 2004.

[19] A. J. Young and C. H. Hansen, "Control of flexural vibration in stiffened structures using multiple piezoceramic actuators," *Appl. Acoust.*, vol. 49, no. 1, pp. 17–48, 1996.

[20] A. Mukherjee, S. P. Joshi, and a. Ganguli, "Active vibration control of piezolaminated stiffened plates," *Compos. Struct.*, vol. 55, no. 4, pp. 435–443, 2002.

[21] V. Balamurugan and S. Narayanan, "Finite element modeling of stiffened piezolaminated plates and shells with piezoelectric layers for active vibration control," *Smart Mater. Struct.*, vol. 19, no. 10, p. 105003, 2010.

[22] A. H. Daraji and J. M. Hale, "Active vibration reduction by optimally placed sensors and actuators with application to stiffened plates by beams," *Smart Mater. Struct.*, vol. 23, no. 11, p. 115018, 2014.

Figure Captions List

Fig.1. Doubly curved shell stiffened by beams and bonded with sensor/actuator pair

Fig. 2. Simulink design based on the optimal linear quadratic control scheme

Fig. 3. Doubly curved composite shell

Fig. 4. Doubly curved composite shell stiffened by four beams located symmetrically

Fig.5. Population fitness progression over 50 generations. Each individual is represented as one of the points distributed around the circle, with its fitness values, obtained from its chromosome, defining its distance from the centre with large radius indication high fitness

Fig. 6. Sensor/actuator placement for the cantilever composite shell. Each dot shows the location of a s/a pair in one of the 100 breeding individuals in each generation. Initially they are randomly distributed. After 10 generations, they have begun to group in efficient locations. After 50 generations, they have completely converged on four optimal sites at the root of the cantilever shell.

Fig. 7. Fitness value for the best individual in each generation repeated for seven times for the cantilever composite shell

Fig.8. Population fitness progression over 100 generations for the composite stiffened shell. Each individual is represented as one of the points distributed around the circle, with its fitness values, obtained from its chromosome, defining its distance from the centre.

Fig. 9. Sensor/actuator placement for the stiffened composite shell mounted rigidly from the four side edges. Each dot shows the location of a s/a pair in one of the 100 breeding individuals in each generation. Initially, they are randomly distributed. After 20 generations, they have begun to group in efficient locations. After 100 generations, they have completely converged on four optimal sites.

Fig. 10. Fitness value for the best individual in each generation repeated for seven times for the stiffened composite shell

Fig. 11. Electric field distribution at the first and third modes for the stiffened composite shell bonded with full coverage of single sensor

Fig. 12. Sensor voltage distribution at the first and third mode for the stiffened composite shell bonded with full coverage of single sensor

Fig. 13. Sensor voltage distribution at the first and third mode for the stiffened composite shell bonded with full coverage discrete 225 sensors

Fig. 14. Cas1 and 2 are optimised and non-optimised, respectively, a location of an actuator (05) excited by an external sinusoidal voltage disturbance at first six modes of the stiffened composite shell

Fig. 15. Transient and steady state voltage time responses of the s/a at the optimal location 01 as a result of applied external sinusoidal voltage on actuator at location 05 at the 1st mode for the stiffened shell

Fig. 16. Transient and steady state voltage time responses of the s/a at the optimal location01 as a result of applied an external sinusoidal voltage on actuator at location 05 at the 3rd mode for the stiffened shell

Fig. 17. Transient and steady state voltage time responses of the s/a at the optimal location 01 as a result of applied an external sinusoidal voltage on actuator at location 05 at the 5th mode for the stiffened shell

Table Captions List

Table 1 Composite shell, stiffener and macro fibre composite sensor/actuator properties

Table 2 Natural frequencies

Table 3 sensor output voltage comparison for optimised and non-optimised

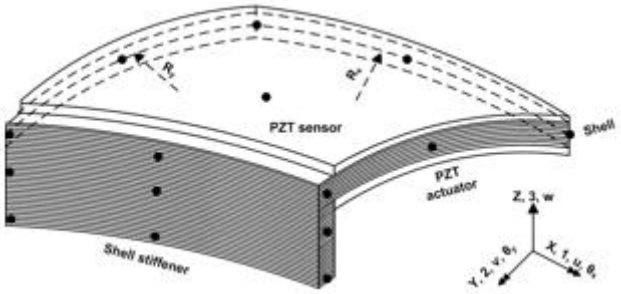

Fig.1. Doubly curved shell stiffened by beams and bonded with sensor/actuator pair

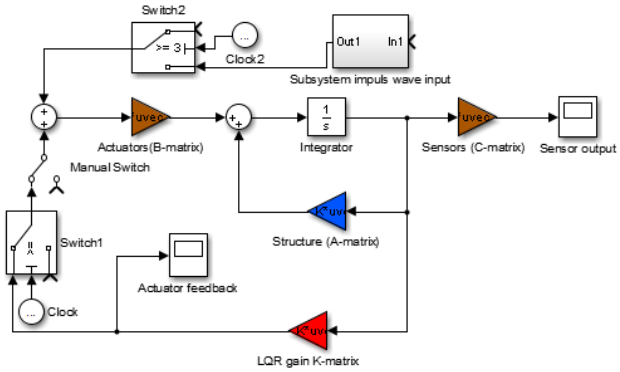

Fig. 2. Simulink design based on the optimal linear quadratic control scheme

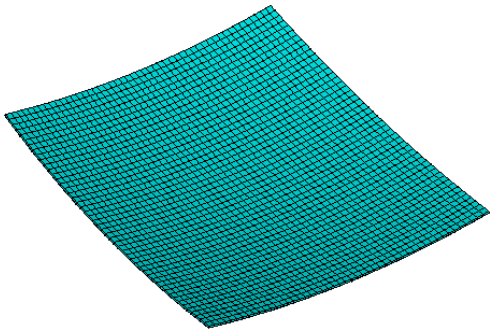

Fig. 3. Doubly curved composite shell

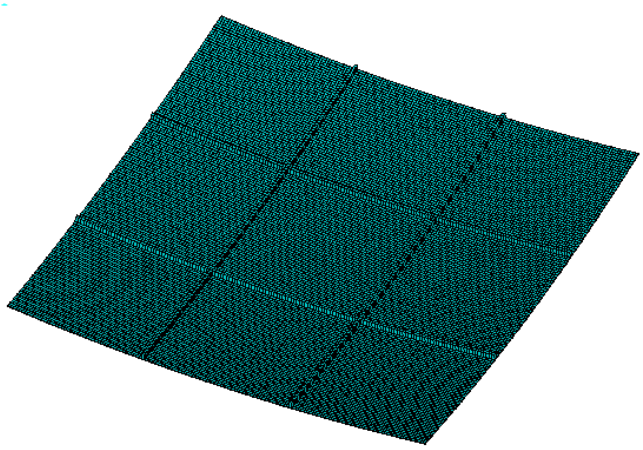

Fig. 4. Doubly curved composite shell stiffened by four beams located symmetrically

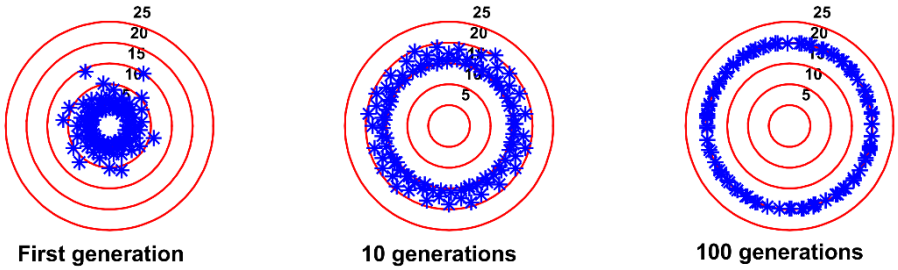

Fig.5. Population fitness progression over 50 generations. Each individual is represented as one of the points distributed around the circle, with its fitness values, obtained from its chromosome, defining its distance from the centre with large radius indication high fitness

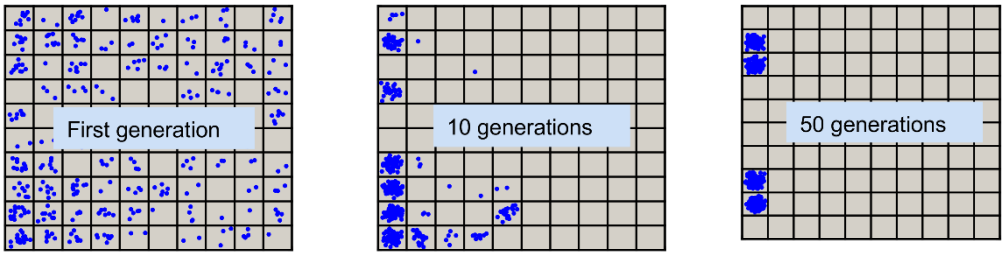

Fig. 6. Sensor/actuator placement for the cantilever composite shell. Each dot shows the location of a s/a pair in one of the 100 breeding individuals in each generation. Initially they are randomly distributed. After 10 generations, they have begun to group in efficient locations. After 50 generations, they have completely converged on four optimal sites at the root of the cantilever shell.

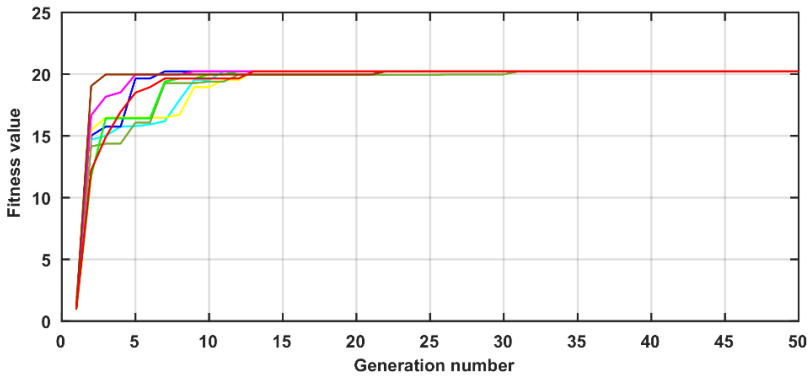

Fig. 7. Fitness value for the best individual in each generation repeated for seven times for the cantilever composite shell

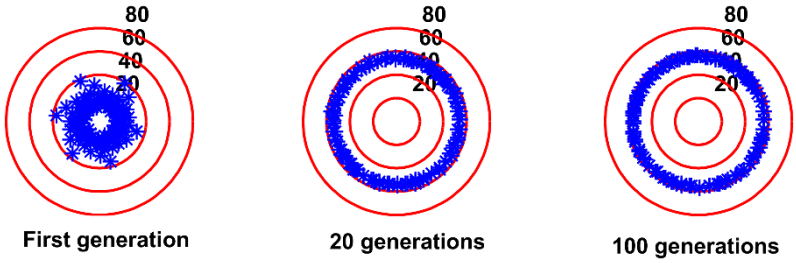

Fig.8. Population fitness progression over 100 generations for the composite stiffened shell. Each individual is represented as one of the points distributed around the circle, with its fitness values, obtained from its chromosome, defining its distance from the centre.

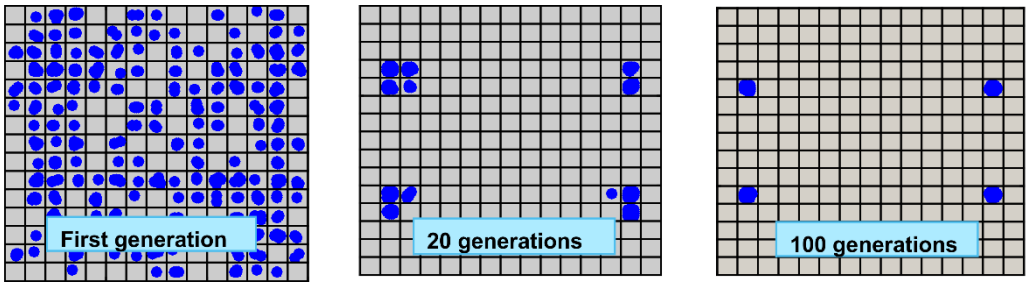

Fig. 9. Sensor/actuator placement for the stiffened composite shell mounted rigidly from the four side edges. Each dot shows the location of a s/a pair in one of the 100 breeding individuals in each generation. Initially they are randomly distributed. After 20 generations, they have begun to group in efficient locations. After 100 generations, they have completely converged on four optimal sites.

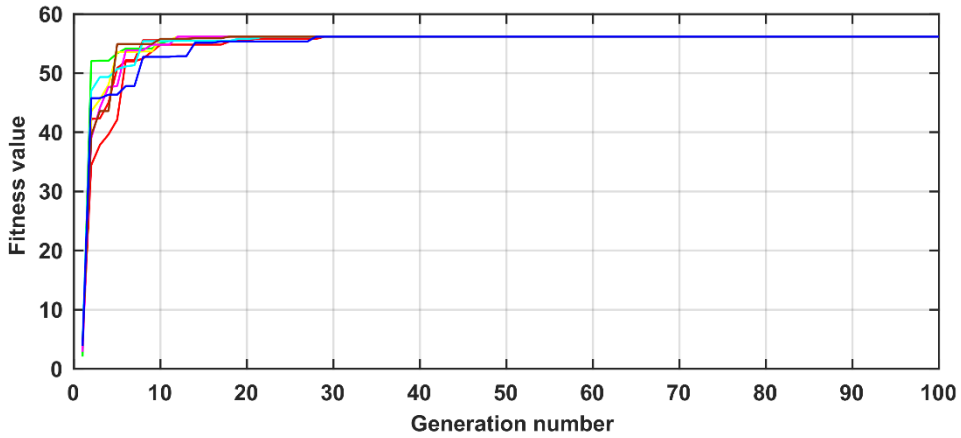

Fig. 10. Fitness value for the best individual in each generation repeated for seven times for the stiffened composite shell

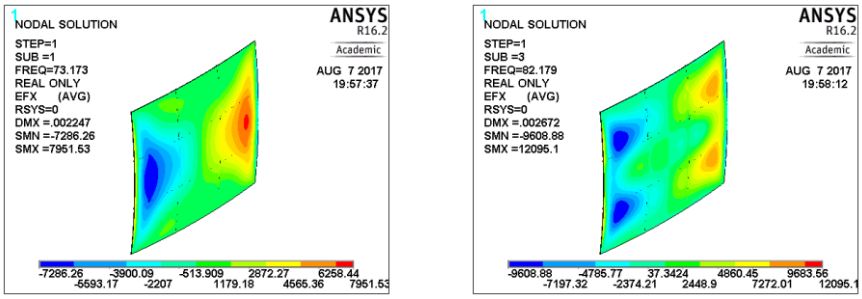

Fig. 11. Electric field distribution at the first and third modes for the stiffened composite shell bonded with full coverage of single sensor

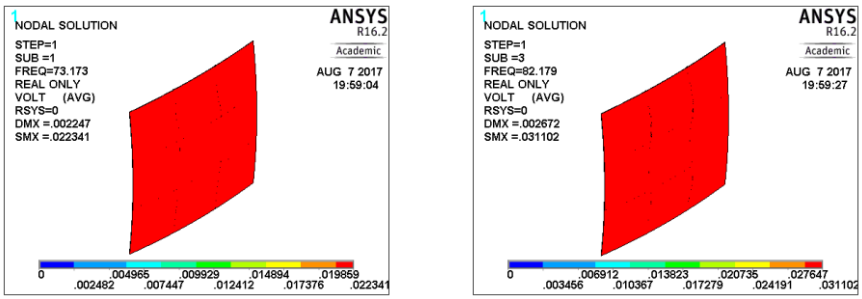

Fig. 12. Sensor voltage distribution at the first and third mode for the stiffened composite shell bonded with full coverage of single sensor

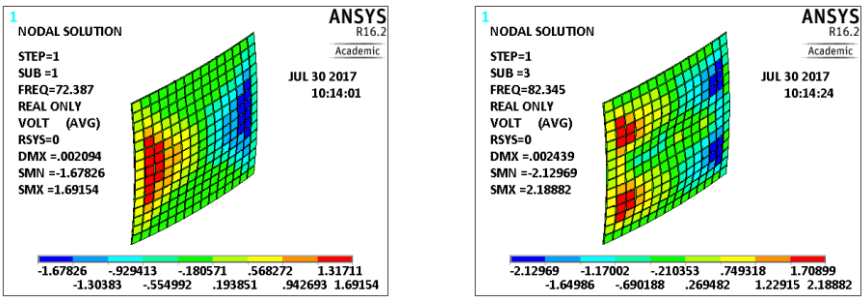

Fig. 13. Sensor voltage distribution at the first and third mode for the stiffened composite shell bonded with full coverage discrete 225 sensors

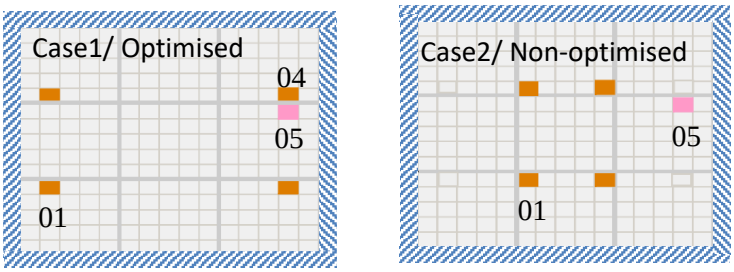

Fig. 14. Cas1 and 2 are optimised and non-optimised, respectively, a location of an actuator (05) excited by an external sinusoidal voltage disturbance at first six modes of the stiffened composite shell

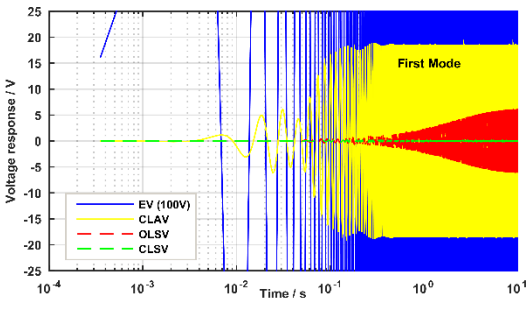

Fig. 15. Transient and steady state voltage time responses of the s/a at the optimal location 01 as a result of applied external sinusoidal voltage on actuator at location 05 at the 1st mode for the stiffened shell

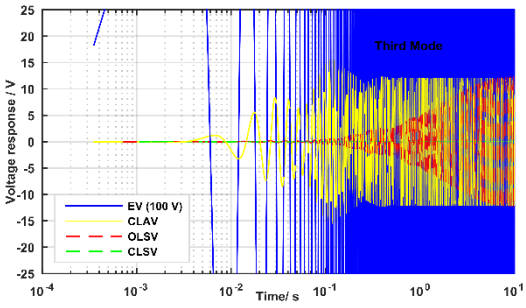

Fig. 16. Transient and steady state voltage time responses of the s/a at the optimal location01 as a result of applied an external sinusoidal voltage on actuator at location 05 at the 3rd mode for the stiffened shell

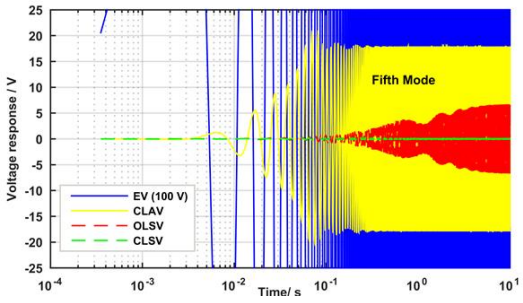

Fig. 17. Transient and steady state voltage time responses of the s/a at the optimal location 01 as a result of applied an external sinusoidal voltage on actuator at location 05 at the 5^{th} mode for the stiffened shell

Table 1 Composite shell, stiffener and macro fibre composite sensor/actuator properties

Properties	Shell	Stiffened shell	stiffeners	MFC type d31
E_x, E_y, E_z (GPa)	51.76, 46.54, 9.68	same	same	---------
G_{xy}, G_{yz}, G_{xz} (GPa)	4.945,4.945,14.27	same	same	---------
$\mu_{xy}, \mu_{yz}, \mu_{xz}$	0.475, 0155, 0.153	same	same	---------
Density (Kg/m^3)	1540	same	same	7000
R_x, R_y (mm)	1500	6500	6495	6503
Dimensions (mm)	500×500×3	1500×1500×3	1500×10×5	40×40×0.3
e_{31}, e_{32}, e_{33} (C/m^2)	---------	---------	--------	-7.12, -4.53,12.1
$C_{11}^E, C_{12}^E, C_{13}^E, C_{55}^E$ (GPa)	---------	---------	--------	39.4,12.9,8.3,5.5
μ_{33}^{σ} (F/m)	---------	---------	--------	1.27×10^{-8}

Table 2 Natural frequencies

Case	Fundamental frequencies Hz					
	ω_1	ω_2	ω_3	ω_4	ω_5	ω_6
Cantilever composite shell	16.70	17.34	61.92	67.41	99.42	137.23
Cantilever composite shell bonded with four s/a pairs	17.05	17.81	63.43	68.09	100.05	140.24
Stiffened composite shell	72.97	78.92	83.38	85.03	93.50	93.99
Stiffened composite shell bonded with fours s/a pairs	73.10	79.13	83.27	85.58	93.30	94.27

Table 3 sensor output voltage comparison for optimised and non-optimised

Case	Steady state sensor voltage output (V)					
	1st	2nd	3rd	4th	5th	6th
Case1 optimised	6.0	2.8	12.5	10.2	6.7	16.0
Case2 non-optimised	0.15	0.13	3.0	0.14	2.0	0.4